

M.L. YOUNG¹
F. CASADIO²
S. SCHNEPP²
J. ALMER³
D.R. HAEFFNER³
D.C. DUNAND^{1,✉}

Synchrotron X-ray diffraction and imaging of ancient Chinese bronzes

¹ Department of Materials Science and Engineering, Northwestern University, Evanston, IL, 60208, USA

² The Art Institute of Chicago, Chicago, IL, 60603, USA

³ Advanced Photon Source, Argonne National Laboratory, Argonne, IL, 60439, USA

Received: 5 December 2005 / Accepted: 12 December 2005
Published online: 17 February 2006 • © Springer-Verlag 2006

ABSTRACT High-energy synchrotron X-ray diffraction and imaging experiments were performed at the Advanced Photon Source on two ancient Chinese bronzes from the Art Institute of Chicago with the goal to nondestructively study their microstructure. The first object, a bronze fragment from an early Western Zhou dynasty vessel (Hu, 11th/10th century B.C.), was investigated with spatially-resolved diffraction to reveal the depth and composition of the surface corrosion layer as well as the composition and grain size of the underlying bronze core. The second object, a bronze dagger-axe (Ge, 3rd/2nd century B.C.) with a silver-inlaid sheath, was studied under both diffraction and imaging conditions. It was found to have been cast as a single object, answering longstanding scholars' questions on whether the ceremonial object concealed an interior blade.

PACS 81.00; 01.75.+m

1 Introduction

In the past 50 years, the study of early Chinese metallurgy, both from a scientific and archaeological perspective, has grown at an impressive pace. Synchrotron radiation X-ray techniques have the potential to answer specific art-historical questions in a nondestructive way. Uses of synchrotron radiation in archaeometry were reviewed for X-ray fluorescence (XRF) and particle-induced X-ray emission (PIXE) techniques [1] and for XRF, X-ray diffraction (XRD), and X-ray radiography [2]. Since these initial discussions, synchrotron techniques such as micro-XRF and micro-XAS (X-ray absorption spectrometry) have been employed on platinum, iron, and bronze artifacts [3–5]. High-energy synchrotron X-ray diffraction has been used to penetrate thin sections of a bronze fibula originating from the Syrian site of Tell Beydar (3rd millennium B.C.) [6] and more recently ancient brass astrolabes [7, 8].

In this study, we use a third-generation synchrotron source – the Advanced Photon Source (APS), capable of producing a high flux of high energy X-rays (85 keV) – to investigate two objects from the ancient Chinese art collection of the Art Institute of Chicago (AIC). The high brilliance available at

the APS permits the use of small beams for diffraction studies as well as phase-enhanced imaging for higher contrast than traditional X-ray absorption methods. The first object, a bronze fragment from an early Western Zhou dynasty vessel (Hu, 11th/10th century B.C.), was studied in diffraction mode, and results were compared with both compositional results obtained by traditional metallography, first published by Gettens in 1951 [9, 10], and with laboratory X-ray images. The second object, a bronze dagger-axe (Ge, 3rd/2nd century B.C.) with a silver-inlaid sheath, was analyzed in both diffraction and imaging modes. Of particular interest was whether the object contained a blade in its interior, a possibility raised by a prominent scholar of ancient bronze weapons who noted a similarity between the silhouette of the AIC piece and that of a contemporary lacquered wood sheath. Both objects are several millimeters thick and made out of bronze alloys containing several percent of highly absorbent lead, and are thus difficult to study with lower energy X-rays.

2 Experimental set-up

High-energy, phase-contrast X-ray imaging was performed at the 1-ID beam line of the APS, as shown schematically in Fig. 1. The dagger-axe was positioned perpendicular to the beam. Radiographic images were collected using a monochromatic 85 keV ($\lambda = 0.015$ nm) X-ray beam with a square cross-sectional field of view of 2×2 mm². Images were recorded using a charge-coupled-device (CCD) camera, positioned far enough (about 1 m) from the sample to allow for phase propagation (phase-enhanced imaging). For comparison, traditional X-ray imaging was performed at the AIC using a Philips radiographic system operating between 100–320 kV.

The general setup for the diffraction experiments has been described in detail previously [7, 8] and is also shown schematically in Fig. 1. High-energy X-ray diffraction measurements were performed with a monochromatic 85 keV ($\lambda = 0.015$ nm) X-ray beam for exposure times of approximately 60 seconds. The bronze vessel fragment was positioned with its vertical face at a 30° angle relative to the beam, while the dagger-axe was positioned perpendicular to the beam. The X-ray beam for diffraction had a cross-section with 20×200 μm^2 dimensions for the bronze vessel fragment and 200×200 μm^2 for the dagger-axe. Complete Debye–Scherrer

✉ Fax: +1-847-491-7820, E-mail: dunand@northwestern.edu

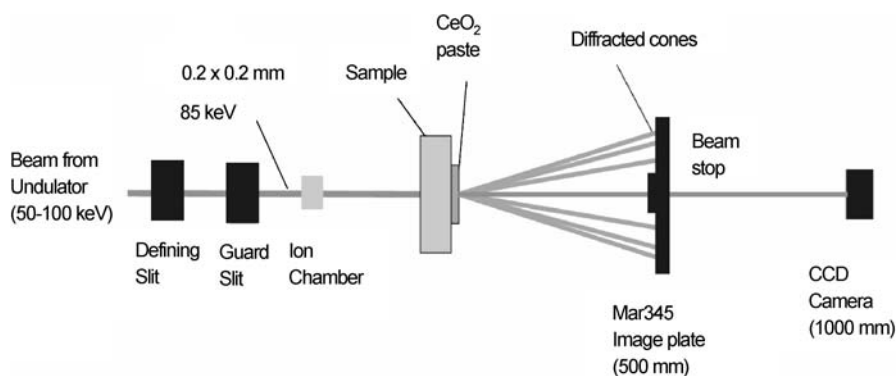


FIGURE 1 Schematic of experimental setup at the APS for combined diffraction and imaging measurements. For imaging, the on-line image plate is removed

diffraction cones from the crystalline phases present in the diffraction volumes were recorded using an on-line image plate. Additional calibration diffraction cones were produced from a paste composed of vacuum pump grease and pure ceria powder, which was contained in a plastic bag placed on the back surface of each object. The on-line image plate (MAR345) had a 345 mm diameter, 100 micron pixel size and 16 bit dynamic range, and the sample–detector distance was 500 mm. The software programs Matlab and Jade were used to create intensity versus d -spacing graphs and for phase identification, respectively.

3 Results and discussion

3.1 Bronze vessel fragment

The thickness of the bronze fragment (shown in Fig. 2a) varies depending upon location, but is on average about 7 mm. A similar bronze fragment originating from the same vessel was originally studied by Gettens in 1951 using traditional X-ray diffraction and metallography [9, 10]. Gettens reported the fragment composition as about 75 wt. % Cu, 20 wt. % Sn, and 5 wt. % Pb. Given that Pb is present as a nearly pure phase [9, 10], the alloy can be considered as a binary Cu–21 wt. % Sn, which should consist, according to the phase diagram, of two phases: a Cu-rich phase consisting of face-cubic-centered Cu with up to 16 wt. % Sn in solid solution, and an intermetallic Sn-rich phase with $\text{Cu}_{41}\text{Sn}_{11}$ composition (33 wt. % Sn). Indeed, Gettens reports from metallographic examination that the uncorroded metal consists of primary copper-rich dendrites within a high-tin phase (whose composition he did not identify), with small lead globules dispersed within the structure.

Traditional X-ray radiographic imaging, as illustrated in Fig. 2b, revealed that the fragment consisted of a collection of sub-fragments held together by a lead-based solder. Gettens [9, 10] reported that the vessel, purchased as a whole object during World War II and of unknown provenance, was in fact a collection of soldered fragments (some ancient and other modern and made of pure copper), with artificial corrosion product made from green-colored stucco used to cover up these repairs. Preliminary observation of the fragments under UV light allowed for clear identification of the repairs and modern decoration motifs, thus simplifying the task of isolating a suitable original area with archaeological corrosion patina to be analyzed with synchrotron X-ray diffraction. Synchrotron X-ray diffraction was performed on a small frag-

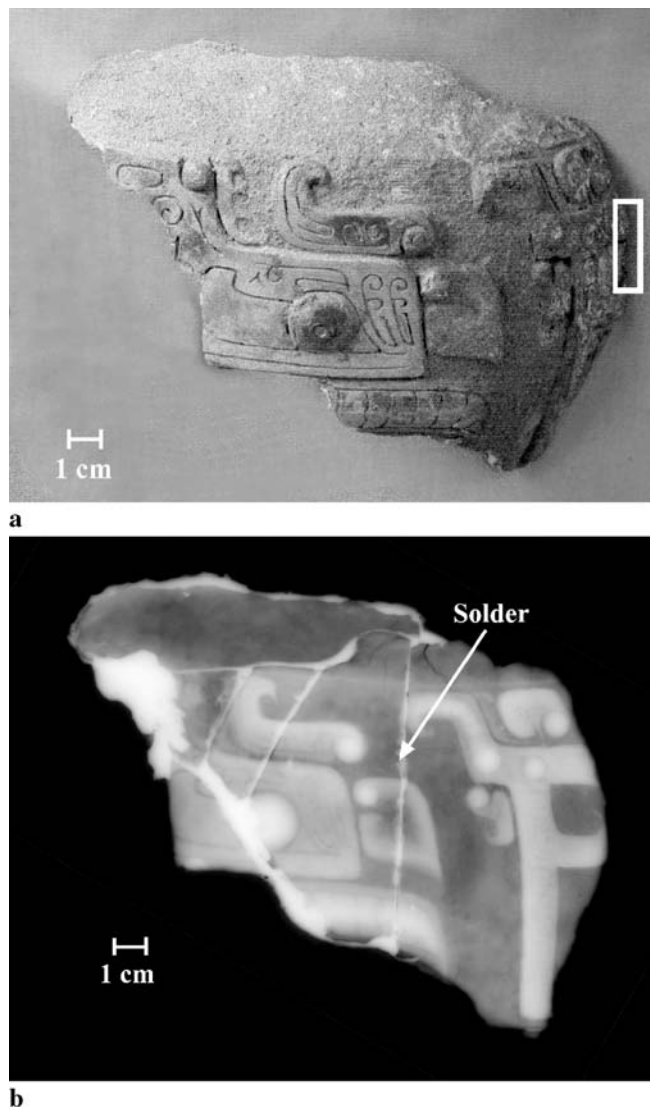


FIGURE 2 Bronze vessel fragment (a) visible light image (courtesy of The Art Institute of Chicago Conservation Laboratory) and (b) a traditional X-ray radiographic image. The box indicates the general area where diffraction was taken (see Figs. 3–4)

ment area (shown in Fig. 2a with a box), where the metal core had been exposed by previous destructive sampling operations, with the goal to compare with results by Gettens and by our own analytical campaign on excised samples from the same area, to assess the nondestructive effectiveness of the

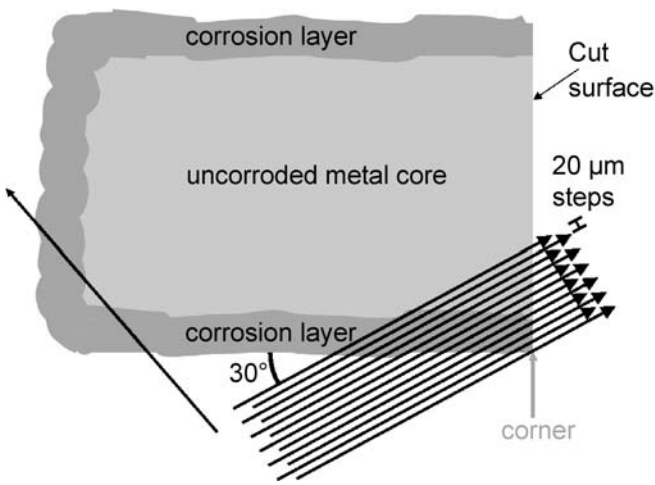


FIGURE 3 Schematic of the bronze vessel fragment position relative to the X-ray beams (*arrow bundle*), not to scale. The *single arrow* on the left shows how the beam could non-destructively probe the corrosion layer in a non-sectioned region

synchrotron technique. As illustrated in Fig. 3, the bronze vessel fragment was rotated so that a $20 \times 200 \mu\text{m}^2$ beam passed through at a 60° angle from the normal to the face of the section. Diffraction patterns were taken in steps of $20 \mu\text{m}$ from the corner of the fragment up to a depth of 1.1 mm . Accounting for the 60° angle, the maximum depth (measured perpendicular to the surface) sampled by the beam was $1.1/(\sin 60^\circ) = 1.3 \text{ mm}$.

In Fig. 4, each spectrum corresponds to the integrated diffraction pattern from a given step, integrated over the full 360° azimuth. By comparing the spectra as a function of sampling depth, it should be possible to determine the ex-

tent of the corrosion layer. The first spectrum ($20 \mu\text{m}$ step) consists entirely, within detection accuracy, of corrosion products: Cu_2O and SnO_2 . In the next several spectra corresponding to the outer edge, the presence of strong peaks for cuprite (Cu_2O) and cassiterite (SnO_2) indicates that the beam is fully contained within the corrosion layer; these two phases were also identified as major phases in the corrosion layer by Gettens [9, 10]. The eleventh spectrum ($220 \mu\text{m}$ total step) exhibits the presence of these two oxides, together with Cu and $\text{Cu}_{41}\text{Sn}_{11}$, which can be interpreted as a metallic core with significant amounts of corrosion products, in agreement with the description by Gettens [9, 10]. At the deepest positions ($> \sim 400 \mu\text{m}$), the peaks from these corrosion products are very weak, but those from the three metallic phases from the original bronze alloy (Cu, $\text{Cu}_{41}\text{Sn}_{11}$ and Pb) are preminent, indicating that the beam is mostly sampling uncorroded material. The depth of the interface between the uncorroded core and the corrosion product is difficult to pinpoint accurately, due to the very similar lattice spacings of metallic and corrosion phases. As is visible in Fig. 4, there is near complete overlap for the following phases: $\text{Pb}(200)/\text{Cu}_2\text{O}(111)$, $\text{Cu}(111)/\text{Cu}_{41}\text{Sn}_{11}(660)/\text{Cu}_2\text{O}(200)$, $\text{Cu}(200)/\text{Cu}_{41}\text{Sn}_{11}(844)$, $\text{Cu}(220)/\text{Cu}_{41}\text{Sn}_{11}(888)/\text{Cu}_2\text{O}(311)$, and $\text{Cu}_{41}\text{Sn}_{11}(16\ 2\ 2)/\text{Pb}(420)/\text{Cu}_2\text{O}(400)$. However, some phase emergences/disappearances can be determined from isolated peaks, such as the $\text{Pb}(111)$ peak which emerges at step-depth of $280\text{--}340 \mu\text{m}$. This Pb emergence is confirmed by looking at subtle differences/peak shifts in the (220), (311), and (420) Pb peaks which overlap with other phases. Another isolated peak, $\text{Cu}_{41}\text{Sn}_{11}(664)$, emerges at a step-depth of about $320 \mu\text{m}$ which is confirmed by the emergence of the $\text{Cu}_{41}\text{Sn}_{11}(14\ 4\ 2)$ peak at about the same position. Moreover, as the $\text{Cu}_{41}\text{Sn}_{11}(14\ 4\ 2)$ peak appears,

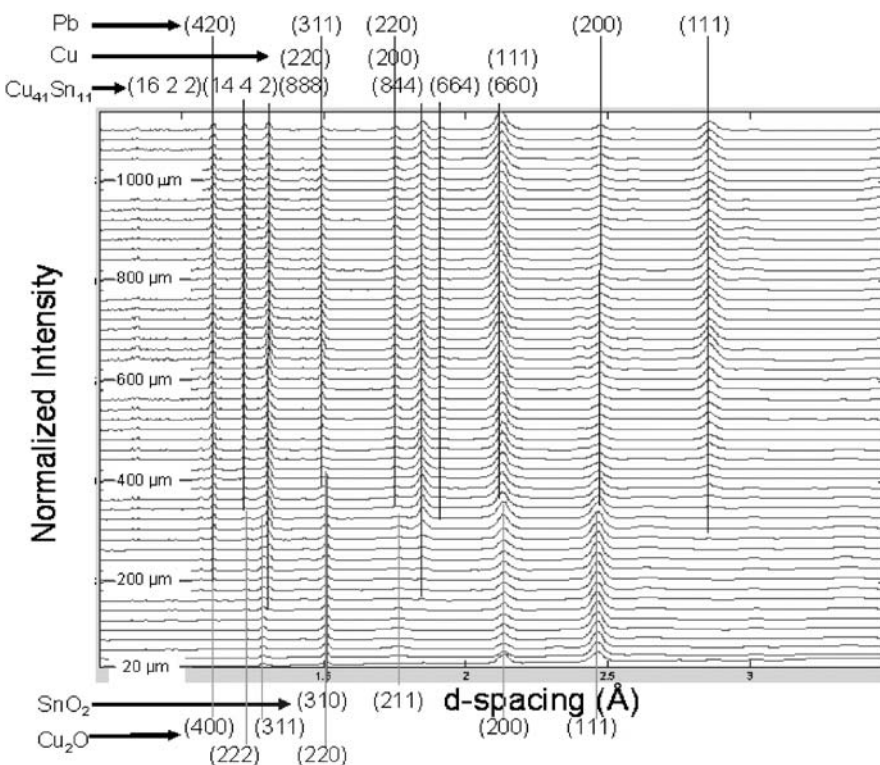


FIGURE 4 Normalized intensity vs. d-spacing for the bronze vessel fragment at fifty-five different positions (distance marked in μm is with respect to corner of fragment, Fig. 3) Beam size: $20 \times 200 \mu\text{m}^2$

the $\text{Cu}_2\text{O}(222)$ peak disappears. These single peak observations are strong evidence that the corrosion layer is about $320/(\sin 60^\circ) = 370 \mu\text{m}$ thick, which is also supported by the disappearance of the $\text{Cu}_2\text{O}(311)$, $\text{Cu}_2\text{O}(220)/\text{SnO}_2(310)$, and $\text{SnO}_2(211)$ peaks at about the same step depth.

Another complication comes from the fact that all Cu peaks overlap with $\text{Cu}_{41}\text{Sn}_{11}$ peaks, but there are a few $\text{Cu}_{41}\text{Sn}_{11}$ peaks at diffraction angles where no Cu peaks are present. It can thus be concluded that $\text{Cu}_{41}\text{Sn}_{11}$ is present, but the presence of Cu is not unequivocally ascertained. However, the Cu phase is less corrosion-sensitive than the $\text{Cu}_{41}\text{Sn}_{11}$ phase which corrodes preferentially leaving pure Cu intact, in the early stages of bronze corrosion [9, 10]; thus, the presence of the $\text{Cu}_{41}\text{Sn}_{11}$ phase guarantees also the presence of the Cu phase.

Based on this study, it can be concluded that the corrosion layer, which is visible optically, is very thin and that the bulk of the fragment is uncorroded, in agreement with cross-sections from Gettens' original publications [9, 10], describing an uncorroded metal core, an intermediate partially mineralized (corroded) zone, and a completely mineralized outer zone. While the sample examined comes from a fragmentary object, it would not be difficult to perform similar diffraction experiments on whole artifacts (provided their thickness does not make collection time prohibitively long) or along a rim, handle or foot of a vessel and other thin-walled object. This would allow for a rapid and nondestructive determination of the thickness of the corrosion layer as well as provide information on the presence or absence of an uncorroded metallic core, which has important implications for the mechanical integrity of the object. Furthermore, identification of crystalline phases by diffraction within the bulk of the corrosion and metal layer can provide precious clues as to the authenticity of the irradiated volume, which extends from one side to the other of the object in the present transmission geometry, rather than a few micrometers in depth as in traditional X-ray fluorescence and diffraction techniques (given the high atomic numbers of Cu, Sn and Pb present in leaded bronze). For example, copper repair pieces and fake corrosion material would be immediately detected.

In addition, other nondestructive synchrotron radiation techniques such as micro-XRF or micro-XRD could aid in more accurately and quantitatively determine all the corrosion products present [2, 3, 5, 6, 11], as some Sn and Cu corrosion products may be poorly crystallized and thus difficult to detect [12–15].

The cuprite and cassiterite phases produce thin, continuous diffraction rings, which are clearly visible in Fig. 5a (pattern taken near the corner) and more faintly in Fig. 5b (pattern taken at near maximum depth). This indicates that a large number of oxide grains are in the diffraction condition, i.e., that the grain size of these phases is much finer than the beam size; it is indeed expected that corrosion products are fine-grained. By contrast, the three metallic phases produce a small number of large diffraction spots (Fig. 5b), indicating a much coarser grain size. Gettens metallographic study indeed shows very coarse Cu dendrites (up to 0.7 mm), but does not provide grain size information for the $\text{Cu}_{41}\text{Sn}_{11}$ or Pb phases. It is thus apparent that synchrotron diffraction studies can provide information on the grain size in a nondestructive manner, and in



FIGURE 5 Synchrotron X-ray diffraction patterns (half of image plate) for the bronze vessel fragment at (a) region near the corner ($100 \mu\text{m}$), where only the diffraction rings from the corrosion layer (a combination of cuprite and cassiterite) are present and (b) the bulk ($1040 \mu\text{m}$) where diffraction spots for the bronze phases (copper, tin-rich, and lead phases) are visible, together with faint corrosion phase rings

the present case confirm that the metallic phase was produced by casting (for which a coarse, untextured grain structure is expected), rather than by cold- or hot-working (with which a fine, textured grain structure is associated).

3.2 Bronze dagger-axe

As shown in Fig. 6, the bronze dagger-axe is T-shaped, with a shaft (vertical in Fig. 6) and two arms (horizontal in Fig. 6). One arm consists of dark-patina bronze with silver inlays, and the second arm of corroded bronze

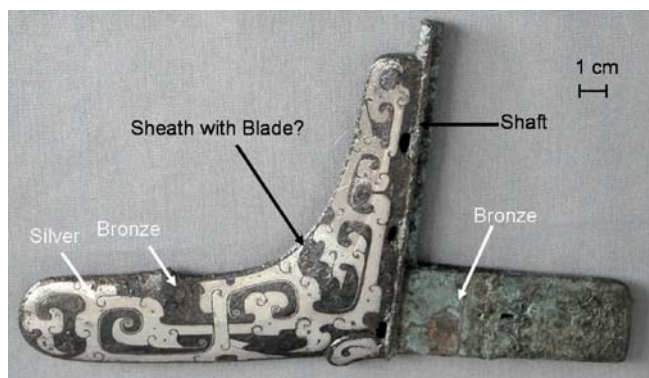


FIGURE 6 Bronze dagger-axe consisting of a bronze arm (right side, corroded, green color) and a thicker bronze arm (left side, with silver inlay) in the shape of a sheath extending from the central shaft. The beam was perpendicular to the image plane. Photo courtesy of The Art Institute of Chicago Conservation Laboratory

(green color), extending into the central shaft which, in its thinnest part, would originally have been inserted into a wooden pole. The bronze/silver arm, which is thicker than the corroded pure bronze arm, has the shape of a sheath; in particular it has a blunted tip. The art-historical question is whether the dagger-axe consists of a functional bronze/silver sheath containing a corroded bronze blade (which cannot be currently removed without damage), or whether the whole object was cast as a single bronze piece (with silver inlays added after casting) to resemble a sheathed blade.

Traditional laboratory X-ray radiography revealed large-scale information such as the presence of some silver inlays under the green corrosion layer of the right arm, and the presence of a large void in the middle of the dagger-axe (Fig. 7a). This cavity appears to be a shrinkage pore with hot tearing due to uneven, slow cooling of the thick section of bronze. However, this evidence alone was not considered sufficient to rule out the presence of a blade within the sheath. The phase-contrast, edge-enhanced synchrotron radiation imaging provided micro-scale information with much higher contrast and resolution: Fig. 7b shows that individual dendrites are visible, with their axis perpendicular to the silver-inlaid edge. Such large, oriented dendrites are expected for a slow-cooled object not subjected to subsequent hot- or cold forming, as for a blade.

A comparison of bulk detail resolution, at the same magnification, between traditional X-ray radiography and synchrotron radiography is shown in Fig. 8a and b. Much clearer detail can be seen using phase-contrast, edge-enhanced synchrotron radiation, including the intricate shape of the silver inlay. It was established from a large series of synchrotron radiographic images that no blade was present within the sheath. The large dendrites and the absence of the blade within the sheathed arm confirm that the object was made for ceremonial purposes.

The synchrotron X-ray diffraction patterns shown in Fig. 9a and b were collected while scanning vertically a 1 mm long section with the $200 \times 200 \mu\text{m}^2$ beam. The individual diffraction spots in Fig. 9a were collected over a region (marked A in Fig. 7a) of predominately bronze with a small amount of surface corrosion and no silver inlay. The very large grain size implied by these large diffraction spots confirms that the object was most likely slow-cooled on solidification, as first deduced from the large dendrites seen in the radiographic images (Fig. 7b). The thin rings resulting from polycrystalline silver diffraction in Fig. 9b were collected over a region (marked B in Fig. 7a) with a combination of bronze, corrosion, and silver inlay. The rings are indicative of fine-grain silver, from which it can be deduced that the inlays were mechanically applied onto the bronze object (most probably by hammering) after the casting step. The double

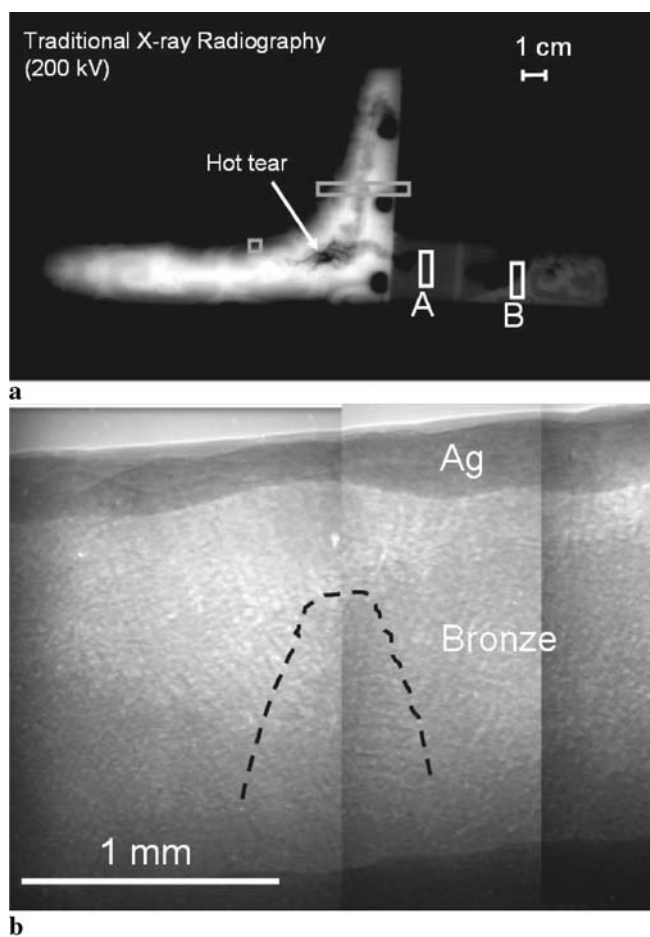


FIGURE 7 (a) Traditional X-ray radiographic image of the dagger-axe showing a large shrinkage pore with hot-tears (arrow). The larger, elongated gray box indicates where the mid-section slice (Fig. 8a,b) originated. The elongated white boxes marked A and B indicate regions where diffraction patterns were taken (Fig. 9a,b). (b) Higher magnification image (acquired by synchrotron radiography) of the edge of the dagger-axe covering the small square box in a. The dashed line outlines the envelope of a dendrite

rings visible in Fig. 9a are due to the fact that silver is inlaid on both faces of the sheath. This illustrates that synchrotron diffraction can be used to study metallic layers buried under corrosion products and separated by several millimeters of bronze.

In summary, observations made from synchrotron X-ray radiography and diffraction provide strong indications that the bronze dagger-axe is a ceremonial object cast in a single block from bronze, and does not contain a bronze blade within a bronze sheath. In the future, X-ray fluorescence could be used in combination with imaging and X-ray diffraction. Furthermore, conical slit system, available at Sector 1 of the APS [16], could be used to provide longitudinal resolution

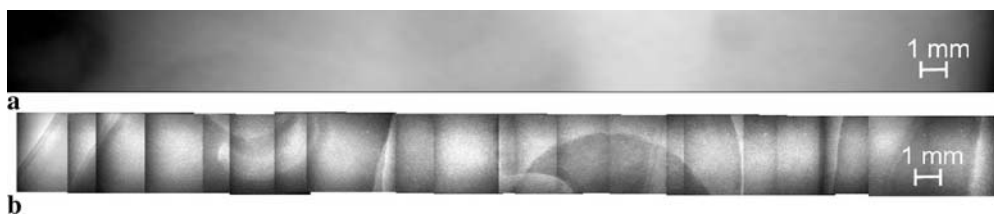


FIGURE 8 (a) Traditional X-ray radiographic image of the mid-section of the dagger-axe (elongated box in Fig. 7a). (b) A composite of synchrotron X-ray radiographic images of the same mid-section of the dagger-axe

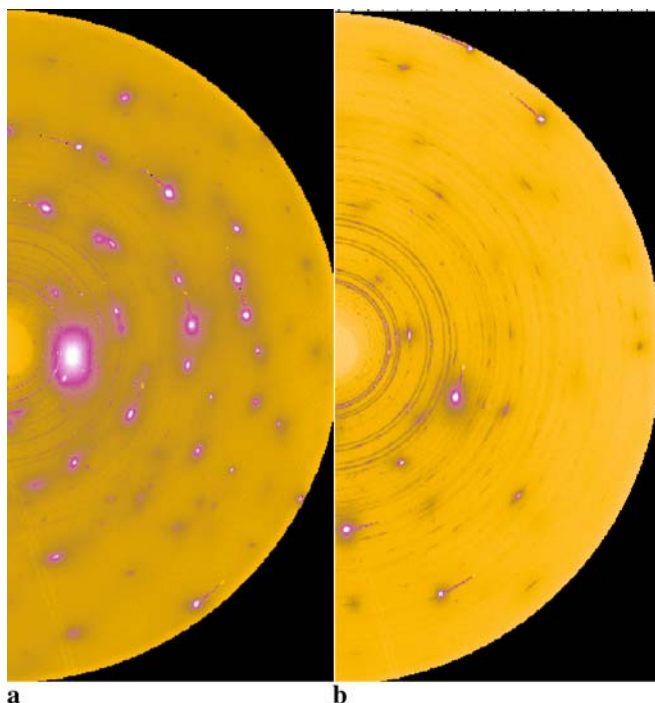


FIGURE 9 Synchrotron X-ray diffraction patterns collected by scanning over $0.2 \times 1 \text{ mm}^2$ regions (A and B in Fig. 7a) consisting of (a) predominantly bronze with a small amount of surface corrosion and no silver inlay and (b) a combination of bronze, corrosion layers, and silver inlay

($\sim 100 \mu\text{m}$) and thus perform 3-D spatially-resolved X-ray diffraction measurements.

4 Conclusions

High-energy synchrotron X-ray diffraction and imaging were performed at the Advanced Photon Source on two ancient Chinese bronzes from the Art Institute of Chicago in an effort to nondestructively answer some longstanding questions.

The first object, a bronze fragment from a early Western Zhou dynasty vessel (Hu, 11th/10th century B.C.), yielded nondestructive information on the composition of the corrosion layer and underlying bronze core, the qualitative grain size of these two regions, and the depth of the interface between them. Similar information was obtained in previous, destructive metallographic studies by Gettens [9, 10]. This feasibility study, offering a unique opportunity to cross-reference and confirm nondestructive, synchrotron X-ray diffraction data with results obtained with conventional, destructive methods of analysis, paves the way to using transmission synchrotron X-ray diffraction to investigate fully-intact museum and archaeological objects. In particular, the possibility to perform depth profiling of corrosion products with $\sim 20 \mu\text{m}$ resolution, and assessing the presence and condition of the metallic core, in nondestructive mode with rapid collection times would allow probing of statistically representative sets of areas in each object and constitutes a great advantage of synchrotron-based techniques. It should be noted that the nondestructive high-energy X-ray diffrac-

tion measurements presented in this paper were performed on a corroded sample which had previously been destructively prepared, thus conveniently exposing the metal core. In general, though, truly nondestructive measurements could be performed on the corrosion layers of intact samples at a grazing angle or at a steeper angle sampling both metal core and corrosion layers, in particular at sharp corners existing in the artifact (such as handles, feet, or sculptural details that project out).

The second object, a bronze dagger-axe from the Eastern Zhou dynasty (Ge, 3rd/2nd century B.C.) with a silver-inlaid sheath was studied in a nondestructive manner by both X-ray imaging and diffraction. It was determined that the sheath does not contain a blade, confirming that the axe was used solely as a ceremonial object. Details within the object could be observed at much higher resolution using phase-contrast X-ray imaging as compared to traditional X-ray radiography. Diffraction showed that the bronze is coarse-grained while the silver is fine-grained, indicating that the bronze axe was most likely cast and slowly-cooled before the silver inlays were hammered into place.

ACKNOWLEDGEMENTS The authors thank the supporting staffs at both the Art Institute of Chicago and the Advanced Photon Source, especially Drs. Wah-Keat Lee and Kamel Fezzaa (APS) for assistance with X-ray imaging. Use of the Advanced Photon Source at Argonne National Laboratory was supported by the U.S. Department of Energy (DOE), Office of Science, Office of Basic Energy Sciences, under Contract No. W-31-109-ENG-38. This research also benefited from the financial support from the Andrew W. Mellon Foundation. Dr. James E. Love is gratefully acknowledged for permission to conduct scientific testing on the Kelley bronze fragments, on loan to AIC.

REFERENCES

- 1 G. Harbottle, B.M. Gordon, K.W. Jones, *Nucl. Instrum. Methods Phys. Res. B* **14**, 116 (1986)
- 2 M. Schreiner, B. Fruhmann, D. Jembrih-Simburger, R. Linke, *Powder Diffr.* **19**, 1 (2004)
- 3 M.F. Araujo, T. Pinheiro, P. Valerio, A. Barreiros, A. Simionovici, S. Bohic, A. Melo, *J. Phys. IV* **104**, 523 (2003)
- 4 D. Grolimund, M. Senn, M. Trottmann, M. Janousch, I. Bonhoure, A.M. Scheidegger, M. Marcus, *Spectrochim. Acta B* **59**, 1627 (2004)
- 5 K. Janssens, G. Vittiglio, I. Deraedt, A. Aerts, B. Vekemans, L. Vincze, F. Wei, I. Deryck, O. Schalm, F. Adams, A. Rindby, A. Knochel, A. Simionovici, A. Snigirev, *X-ray Spectrom.* **29**, 73 (2000)
- 6 A. De Ryck, A. Adriaens, E. Pantos, F. Adams, *Analyst* **128**, 1104 (2003)
- 7 B. Newbury, B. Stephenson, J.D. Almer, M. Notis, G.S. Cargill, G.B. Stephenson, D.R. Haeffner, *Powder Diffr.* **19**, 12 (2004)
- 8 G.B. Stephenson, B. Stephenson, D.R. Haeffner, *MRS Bull.* **26**, 19 (2001)
- 9 R.J. Gettens, *J. Chem. Educ.* **28**, 67 (1951)
- 10 R.J. Gettens, *The Freer Chinese Bronzes*. In *Freer Gallery of Art: Oriental Studies*, No. 7. Smithsonian Institution, Washington (1969) pp. 127–131
- 11 B. Kanngießer, W. Malzer, I. Reiche, *Nucl. Instrum. Methods Phys. Res. B* **211**, 259 (2003)
- 12 I. Constantinides, A. Adriaens, F. Adams, *Appl. Surf. Sci.* **189**, 90 (2002)
- 13 C. Debiemme-Chouvy, F. Ammeloot, E.M.M. Sutter, *Appl. Surf. Sci.* **174**, 55 (2001)
- 14 I. Mabile, A. Bertrand, E.M.M. Sutter, C. Fiaud, *Corros. Sci.* **45**, 855 (2003)
- 15 L. Robbiola, J.-M. Blengino, C. Fiaud, *Corros. Sci.* **40**, 2083 (1998)
- 16 S.F. Nielsen, A. Wolf, H.F. Poulsen, M. Ohler, U. Lienert, R.A. Owen, *J. Synchrotron. Radiat.* **7**, 103 (2000)